Spectral analysis on optimizing X-ray tubes operating parameters and performance for non-destructive material quality analysis

Master's thesis, 2.11.2020

Tekijä:

Jenna Tarvonen

Ohjaaja:

Mikko Laitinen
Mikko Palosaari (Stresstech)

UNIVERSITY OF JYVÄSKYLÄ
DEPARTMENT OF PHYSICS

Abstract

Tarvonen, Jenna
Spectral analysis on optimizing X-ray tubes operating parameters and performance for non-destructive material quality analysis
Master's thesis
Department of Physics, University of Jyväskylä, 2020, 60 pages.

This Master's Thesis was made in cooperation with the University of Jyväskylä and Stresstech Oy. The purpose of this work is to compare the X-ray tubes from two different manufacturers (TruFocus and MRX), to obtain information about the properties and function of tubes and changes in spectra when measuring with different acceleration voltages and currents. The goal is to get results with which to optimize the X- ray diffraction measurements in laboratory work. For this reason, I will also briefly present the diffraction phenomenon and intensity calculations used to analyze the diffraction spectrum in some of the XRD measurements.

Measurements were carried out with tubes of three different target materials, Cr, Cu and Mn from both of the manufacturers and in addition the titanium target tube was tested from TruFocus. The acceleration voltages and currents were selected based to the top limits of each tube as well as the notations made in the laboratory work earlier.

Results were mainly as expected; the intensities of the K_α-peaks increased with increasing voltages and currents. However, with chromium (TruFocus), the 1 kV rise in voltage in the highest range of the values no longer increased the intensity further. In a case of titanium, the bremsstrahlung radiation had significantly higher intensity maxima than the characteristic peaks which is why the exposure times need to be longer to get the signal-to-noise-ratio in acceptable level. Measurements with tubes of manganese and copper targets, and to some extent also chromium, produced unwanted effects like pile-up and secondary radiation which may distort the subsequent analysis of the measured spectra.

In general, TruFocus was more reliable and had better usability when comparing the operational function of the tubes from different manufacturers. However, the

sampling in this thesis was so narrow that additional measurements are needed to confirm the observations.

Keywords: X-ray tube, spectrum, diffraction, intensity corrections

Tiivistelmä

Tarvonen, Jenna
Spektrianalyysi röntgenputkien suorituskyvystä sekä käyttöparametrien optimoinnista ainetta rikkomattomassa materiaalitutkimuksessa
Pro gradu-tutkielma
Fysiikan laitos, Jyväskylän yliopisto, 2020, 60 sivua

Tämä tutkielma on tehty Jyväskylän yliopiston ja Stresstech Oy:n yhteistyönä. Työn tavoitteena on verrata kahden eri valmistajan (TruFocus, MRX) röntgenputkia sekä saada tietoa eri kiihdytysjännitteiden ja virtojen vaikutuksesta putkien toimintaan ja säteilyn spektriin. Tulosten avulla on tarkoitus optimoida käytännön röntgendiffraktio- mittauksia laboratoriossa, jonka vuoksi esittelen lyhyesti myös diffraktioilmiötä sekä sen spektrin intensiteettiin vaikuttavia tekijöitä.

Mittaukset tehtiin molempien valmistajien kolmea eri kohtiomateriaalia sisältävillä putkilla (Cr, Cu, ja Mn) sekä lisäksi TruFocuksen titaani-kohtio putkella. Kiihdytysjännitteet ja virrat valittiin kunkin putken ylärajojen sekä aiempien mittaushavaintojen perusteella.

Tulokset olivat pääosin odotetunlaisia; K_α- piikkien intensiteetit kasvoivat jännitteiden ja virtojen kasvaessa. Poikkeuksina kromilla 1 kV:n nousu ylärajan tuntumassa ei vaikuttanut piikin intensiteettiin eikä muotoon ja toisaalta titaanilla jarrutussäteilyn voimakkuus ylitti selvästi karakteristisen piikkien voimakkuuden ja valotusaika olikin oltava pidempi riittävän resoluution aikaansaamiseksi. Mangaani- ja kupari- sekä jossain määrin myös kromi-kohtioisten putkien mittauksissa oli havaittavissa haitallisia ilmiöitä kuten "pile-upia" ja sekundäärisäteilyä, jotka voivat vääristää spektrin jatkoanalysointia.

Toiminnallisesta näkökulmasta TruFocus oli varmempi, mutta otannan ollessa varsin pieni, lisää mittauksia tarvitaan asian varmistamiseksi.

Avainsanat: Röntgenputki, spektri, diffraktio, intensiteettikorjaukset

Preface

The practical work for this thesis was carried out in Stresstech Oy in autumn 2019. I would like to express my sincere thanks to my co-workers in the measurement laboratory and to my supervisor Mikko Palosaari for the help and guidance planning and implementing the measurements. A massive thanks to my close friends Henri Larjosuo and Aapo Tamminen for the encouragement during the process and for the latter also thanks for the coding advice with Octave.

My other supervisor Mikko Laitinen, I'm grateful for your encouragement and valuable advice. Thank you also for answering and making the correction notes even on your vacation when you knew the schedule was tight.

Special thanks to my family and friends for all the support. Sorry I haven't been present in all the situations I would have wanted to be. Finally, thank you Kari, for all the encouragement and support, in both good and bad moments.

Jyväskylässä 2. marraskuuta 2020

Jenna Tarvonen

Contents

1 Introduction

In November 1895 Wilhelm Conrad Röntgen discovered the existence of X-rays in his laboratory at the University of Würzburg. His experimental setup corresponded to the first X-ray tube which was used to penetrate the material and project image of it onto the film.[1] Therefore, the earliest applications were mainly in medical science. Already Röntgen's research showed that the absorption of X-rays strongly depends on the atomic number of the material.[2]

The next significant step in 1912 was diffraction of X-rays. The discovery opened the doors to investigation of crystal structured materials in atomic level and also proved that X-rays are a short wavelength electromagnetic radiation. In the same year W.D. Coolidge developed a new type of X-ray tube, where heating the filament causes an electron emission which is accelerated to the water-cooled anode.[2] Accelerated electrons produce the typical X-ray spectrum with bremsstrahlung radiation and material specific characteristic peaks. Nowadays, crystallographic material structure investigation with X-ray diffraction is based on the separation and identification of these peaks.

In this thesis I will study how the X-ray spectrum changes when measuring with different acceleration voltages and currents and which would be the most optimal parameters for signal-to-noise-ratio and peak intensity. In addition, I will briefly investigate the diffraction phenomenon and introduce the intensity corrections which are important when analyzing the X-ray diffraction results.

K_α-peak occures in the X-ray spectra when the excitation of the atom is discharged from an adjacent energy state. Produced radiation is called characteristic because of the wavelength, and since also the energy, is characteristic to the certain material. In XRD measurements the K_α-peak is used to identify and observe the composition and properties of the material.

One of the most important products of Stresstech Oy are goniometers based on the XRD technology. Equipment are tested and also quality control measurements are done in the laboratory of Stresstech. Improving the signal-to-noise-ratio of the characteristic K_α-peak allows the investigation of more heterogeneous materials.

Optimizing the measurement parameters and conditions as well as choosing the high quality tubes are important aspects in this case and are the main motivation to carry out these measurements.

Measurements were done tubes with four different target materials and from two different manufacturers. One of the topics of this thesis was also to compare the usability and efficiency of the two types.

2 Electromagnetic radiation, its properties and interactions with matter

In this section I briefly introduce the basic theory of electromagnetic radiation and its interactions with matter. In addition, I go through the basic principles and concepts about photon attenuation in material.

2.1 Electromagnetic radiation

According to the quantum based theory electromagnetic radiation has a dual wave-particle character. This means that explaining its various phenomena, sometimes the wave concept and sometimes particle concept is needed.[3]

Electromagnetic radiation can be seen either as a wave of synchronized oscillations of electric and magnetic fields or a stream of pulses of particles which are propagating perpendicular to the direction of radiation. Particles, called quanta or photon, can for example be produced by emission when an excitation state in an atom discharges. Here, the energy of the emitted photon is quantized and depends on the source of the emission. For example high energy gamma- rays are a consequence of nuclear events while radiowaves with low energy and frequency are produced in oscillations of electrons. However, this is a rough generalization and different regions of the electromagnetic spectrum, Figure 1, do overlap. [4, 3]

Quantized energy of the photon, E, is proportional to its frequency f according to the equation

$$E = hf = \frac{hc}{\lambda} , \tag{1}$$

where h is Planck's constant, c speed of light and λ is the wavelength of the photon.[3]

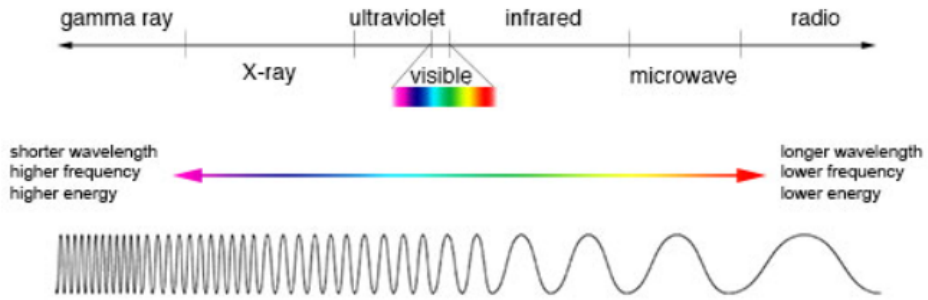

Figure 1. Electromagnetic spectrum and variation of wavelength, frequency and energy.[5]

2.2 Attenuation and the quality of the photon beam

While traveling through the matter, radiation loses its energy in interactions with atomic electrons and nucleus. It is said, that radiation attenuates, meaning, its intensity decreases inversely with the square of the distance. [6] There are several types of interactions, four of which are most relevant to this thesis will be discussed in the following chapters.

The fraction of the incident and the attenuated intensity depends on the properties of the radiation and the target material. Let's consider a monoenergetic, parallel photon beam for which the exponential attenuation law can be written

$$I(x) = I_0 e^{-\mu(hf,Z)x}, \tag{2}$$

where I is the attenuated and I_0 the incident intensity, x is the thickness of the homogenous target material and μ is the linear attenuation coefficient which depends on the photon energy and the atomic number of the target. Attenuation over a certain distance x depends on the number of electrons i.e the density of the material. By dividing the coefficient with density the resulting mass attenuation coefficient μ/ρ is independent of the density. This coefficient is more practical and therefore more fundamental than the linear attenuation coefficient.[7, 8]

Cross section, σ, quantifies the probability of interaction between two particles. It depends on the type of a radiation and its energy and also a character of a target material. Different interactions dominates in different energy regions and the total cross section, $\sigma_{total} = \sum \sigma_i$, varies accordingly since it is a sum of all the coefficients,

σ_i, from individual interaction types.[7]

The total cross section is related to the mass attenuation coefficient and this relation can be expressed

$$\mu/\rho = \frac{\sigma_{total}}{uA} \ , \tag{3}$$

where u is the atomic mass unit and A is is the mass number of the target material.[7]

2.3 Photon interactions with matter

Particle can transfer the whole or part of its energy to the matter by a single interaction. Photons are uncharged and massless particles and they form a radiation that is indirectly ionizing by liberating directly ionizing particles while traveling through the matter. There are five main types of photon interactions. One of these, photodisintegration, occures only with very high energies (over 10 MeV) and therefore is irrelevant for this thesis. The other four are photoelectric absorption, Rayleigh scattering, Compton scattering and pair production. These are illustrated in Figure 2.[7]

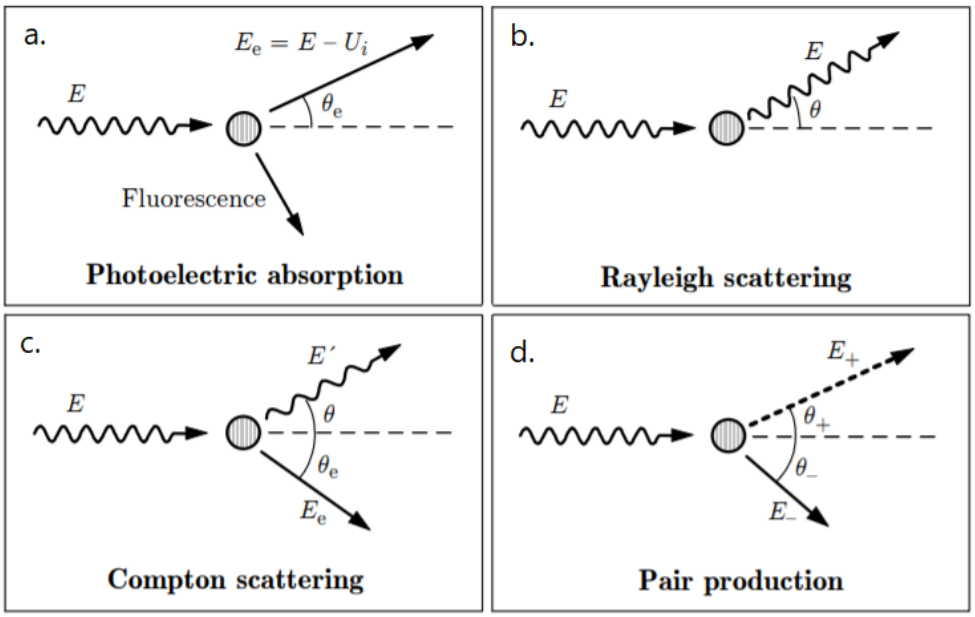

Figure 2. The four main types of photon interactions with matter. E is the energy of the incident photon, U_i is the binding energy and E_e kinetic energy of the emitted electron. Edited from [9].

2.3.1 Photoelectric effect

In the photoelectric effect, a. in Figure 2, the photon is absorbed by a tightly bound orbital electron which is then ejected from the atom. The kinetic energy E_e of the emitted electron is the difference between the incident photon energy E and the binding energy U_i of the electron. This process is most probable when the energy of the photon is equal or just slightly higher than the binding energy of the electron. After the emission of the photoelectron, excitation of the atom is discharged by filling the empty vacancy with an electron from the higher orbital. In this process characteristic X-ray, also called fluorescent radiation, is released. This kind of process can take place with electrons in K, L, M and N atomic shells where K is the lowest and N is the highest in energy respectively.[7, 8]

2.3.2 Rayleigh scattering

Rayleigh scattering, b. in Figure 2, also called as a classical or coherent scattering occurs mostly with interactions between low energy photons and high atomic number material. The process is easiest to visualize by considering an electromagnetic wave of photons passing near the outer orbital electron. Electron starts to vibrate and reradiate energy at the same frequency and wavelength as the incident beam. So there is no ionization or excitation of the target atom, only the direction of the incoming photon is changed.[10]

2.3.3 Compton scattering

When the energy of the photon is high compared to the binding energy of the electron, Compton scattering, c. in Figure 2, becomes the most probable interaction. It can be considered as a collision of the photon and a free electron. Electron receives part of the photon's energy and is emitted at some angle θ while the photon changes its direction to a different angle ϕ. Also the wavelength of scattered photon changes.[11, 8]

Compton effect was observed by Arthur Holly Compton in 1923 and discovery brought a nobel prize for him in 1927. The effect has been important proving the dualistic nature of electromagnetic radiation.[11]

2.3.4 Pair production

Photon interacts with the electromagnetic field of a nucleus and gives up all of its energy in the process called pair production, d. in Figure 2. In the process an electron-positron pair is created and emitted from the atom. The rest mass energy of the electron is 0.51 MeV so the threshold energy for the pair production is 1.02 MeV. If the photon's energy is higher, the excess goes to the kinetic energies of the created particles.[11, 8]

2.4 Electron interactions with matter

Unlike photons, electrons have a mass and a charge and they interact with matter via Coulomb forces. Depending on the energy of the incident electron and the type of the interaction, the result can be either excitation, ionization or emission of radiation.

Inelastic collisions with orbital electrons cause ionization and excitation of the atom. Process is most typical in low atomic number materials. With heavier atoms the probability of interaction with the nucleus increases. In this process the path of the electron is deflected by the positively charged nuclei and the loss of the kinetic energy is directly emitted as an electromagnetic radiation called bremsstrahlung. This process is described in more detail in next section. [12, 8]

In elastic collisions, where kinetic energy is conserved, electrons scatter either from orbital electrons or nuclei. In these processes the direction of the scattered electron is modified by the Coulomb forces.[12, 8]

3 X-Ray

X-ray is electromagnetic radiation with energies approximately from 100 eV to 50 keV[13] and it can result from many different processes such as certain types of radioactive decay to bending the electron beam in synchrotron. X-rays differ from gamma radiation in its mode of origin. While gamma is produced in nuclear reactions, X-rays are always the results of an electronic processes in an atom.[7] This section goes through the basic theory related to X-ray radiation.

3.1 Emission spectrum

When a flux of electrons impact with a material they are decelerated and the kinetic energy is converted to other forms of energy. Collisions with atomic electrons produce heat, but a small amount, usually less than one percent, of the incident electrons comes within a proximity of a nucleus, a suitable distance for the X-ray production[4]. Electron's path is changed in the interaction as discussed in the previous section 2.4, and the loss of kinetic energy is converted to X-ray photons with equal energy. This type of radiation is called a bremsstrahlung radiation.[12]

After the collision of the electron and the bulk atom, the energy of the emitted radiation depends not only on the energy of the incident electron but also the distance between the electron and the nucleus. This dependence occurs because the Coulombic force is proportional to the inverse of the square of the distance. If the electron loses all of its energy in one direct impact, the bremsstrahlung radiation gets the highest value possible, this is called the endpoint energy.[7]

The radial interaction distance defines the probability of the interaction between the electron and the nucleus. Larger circumferential interaction area provides a larger possibility of interactions but the energy of the produced radiation decreases as stated above. This inverse linear relationship between the number of occured interactions and the energy of the X-ray is called the unfiltered bremsstrahlung spectrum. In practical applications, however, spectrum is usually filtered which means that some of the X-rays are removed by attenuation in materials of the device.

A typical X-ray tube, for example, produces radiation from about 5-10 keV, then the intensity increases approximately to one third to one half of the maximal energy and decreases to zero when energy reaches the endpoint. This is illustrated in the Figure 4. [12]

When the energy of the colliding particle exceeds the ionization energy of the target, discrete energy lines, called characteristic peaks, can appear in the spectrum. Electrons, or photons, with energy equal or above the difference between two atomic orbitals, can ionize the atom as previously described in section 2.4. Each peak corresponds to one transition between the levels and is therefore characteristic for the material. With some simplifying assumptions, an approximate formula for the energy of the characteristic peaks can be written

$$\sqrt{f} = C(Z - \sigma) \ , \tag{4}$$

where C and σ are constants. This Moseley law, named after its inventor Henry Moseley, is derived from the large number of experimental data but is also a direct result of the calculations of possible energies of the so called hydrogen-like atoms. According to the law the square root of the frequency, f, is directly proportional to the atomic number, Z, of the target material.[14]

Spectrum can contain several characteristic peaks depending on what kind of electron transition occurs. A subscript of α or β indicates whether the vacancy is filled from adjacent or nonadjacent shells. For example if a vacancy in K - shell is filled with electron from adjacent L - shell, a K_α-peak is produced. Transition from higher M - shell produces K_β-peak which is more energetic but less intense than K_α. Schematic illustration of electron transitions in Figure 3. [14]

A small amount of quantum mechanics is needed for understanding the difference between $K_{\alpha 1}$- and $K_{\alpha 2}$-peaks which can also be seen in the X-ray spectrum in some cases. Every orbital electron has their own unique combination of quantum numbers that describes the energy state and the shape of the orbital. When three of the four quantum numbers are the same but the spin number differs, the spectrum can contain a $K\alpha - doublet$. However, the line is so narrow, value of wavelength ranging 0.38 - 0.50 nm for Z = 28 to 92, that with standard spectrum analysis equipment lines are not usually resolved.[14] An example of unfiltered spectrum with $K\alpha - doublet$ and K_β-peak is illustrated in Figure 4.

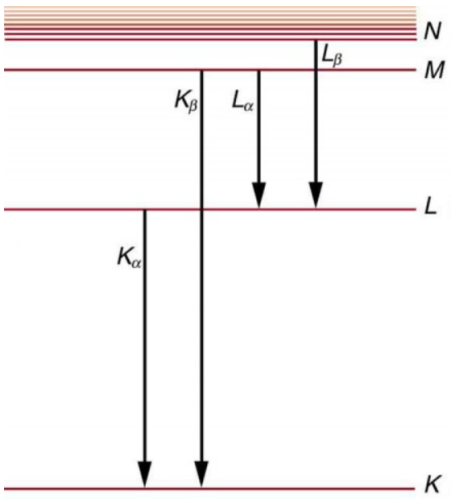

Figure 3. Production of characteristic radiation in different electron transitions from different energy levels.[15]

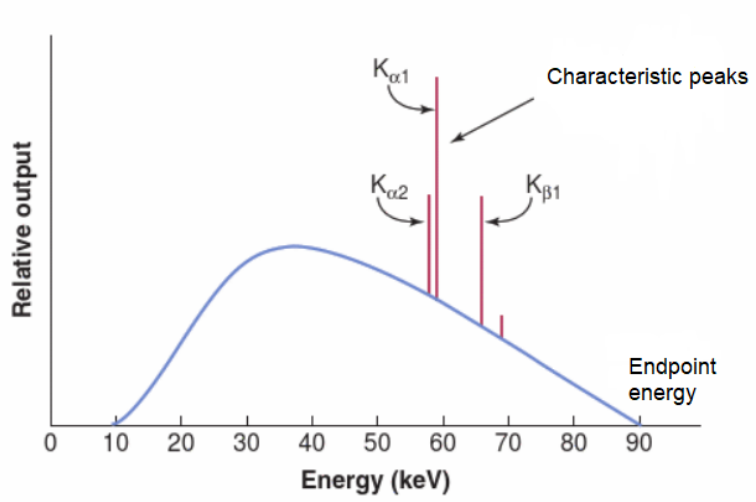

Figure 4. Schematic figure of the X-ray spectrum for Tungsten with 90 kV acceleration voltage. Edited from [12].

3.2 Radiation sources

As noted in the previous section, the X-ray radiation is due to either ionisation of the inner shells of atoms or deceleration of the charged particles in the Coulombic field. Along with the natural sources, several different applications have been developed to create these circumstances. In this subsection I mainly concentrate to introduce the principle of X-ray tube but will also briefly mention a few other sources of X-ray radiation.

3.2.1 X-ray tube

In X-ray spectrometry one of the most common radiation sources is X-ray tube which basic structure is shown in Figure 5. X-ray tubes contain two electrodes placed inside a vacuum housing. The cathode is traditionally a spiral filament, usually made of tungsten because of its properties like heat resistance. The anode is a block of target metal. Heating the filament causes electron emission and electrons are then drawn to the anode due to the potential difference between the electrodes. Hitting to the target decelerates the electrons causing the X-ray photon emission, more precisely the bremsstrahlung. In addition, a fraction of these electrons ionize the target atoms producing characteristic radiation. Emission occurs in all directions but in practical applications it is typically allowed to escape from the tube through only one vacuum tight window. These exit-windows are often made of beryllium which low atomic number provides both vacuum tightness and high transparency to X-rays. Along with the X-ray radiation, considerable amount of heat is formed in the anode. That's why the tube usually contains a cooling system to ensure its reliable and continuous operation.[16, 14]

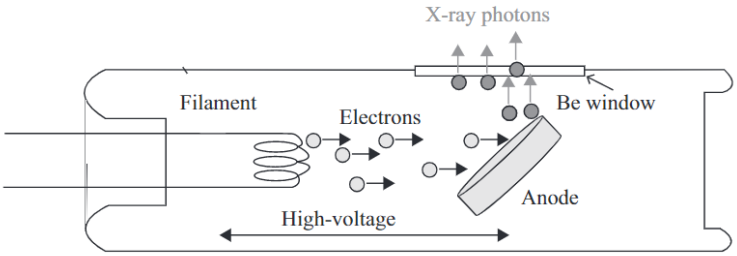

Figure 5. The basic structure of a X-ray tube with a beryllium window.[16]

The heating current applied on to the filament determines the intensity of the

electron flow and thereby the intensity of the produced X-ray spectrum. On the other hand the kinetic energy of the electrons is due to the accelerating voltage and the effect of increasing voltage is seen as an extension of the entire spectrum.

The Equation 1 for photon energy presented earlier can also be applied to express the relation between the electron's energy E_e, acceleration voltage V and the produced X-ray photon

$$E_e = eV = hf = \frac{hc}{\lambda} , \tag{5}$$

where e is elementary charge of the electron.[16, 14]

The applied anode material and the acceleration voltage determines what kind of atoms can be excited with the produced radiation. The emitted X-ray photon must have energy high enough to excite the atoms in the material under study. Therefore, when planning the X-ray diffraction measurements, the selection of the right tube and the measurement parameters is essential.

3.2.2 Other sources

Also a flux of ions can be used to produce X-rays. Due to their large mass compared to electrons, ions interact with the atom as a whole and the energy of deceleration goes to one or more electrons in the atom. Both, bremsstrahlung and characteristic radiation are formed.[14]

In synchrotrons electrons are accelerated with electric field and their path is bent by a strong magnetic field in a circular orbit producing continuous bremsstrahlung radiation. Flux of the radiation can be high in comparison with the X-ray tube since all the electrons moving along the orbit are emitting and also the current is considerably larger. The flux density in synchrotron is also optimized due to the small solid angles while in X-ray tube the emission is almost isotropic.[14]

Radioactive isotopes are also used in X-ray production. Isotopes are generated in cyclotrons or nuclear reactors and can emit characteristic and/or bremsstrahlung radiation at a few different nuclear reactions like internal conversion or α- and β-breakdown processes.[14]

In high temperature plasma the most probable energy for the particle is of the order of 10 keV which is enough to ionize the atom. These processes occur spontaneously in stars but also applications using magnetic and electric fields to

control the plasma has been developed. Heating the plasma with a different types of laser systems and microwaves are also under experiments.[14]

3.3 Absorption of the X-ray

Absorption of the X-ray photon can be divided in two mechanisms, scattering from the electrons of the target atom and the real absorption. Latter consists of fluorescence radiation among others, which corresponds to the characteristic radiation, caused by photoelectric effect or the Auger electron emission. Also heat is always produced during the interaction.[17, 10]

3.3.1 The real absorption

Absorption of the X-ray photons while encountering the matter can be considered using the mass attenuation coefficient. Figure 6 illustrates the dependence between mass attenuation coefficient and photon energy.[2]

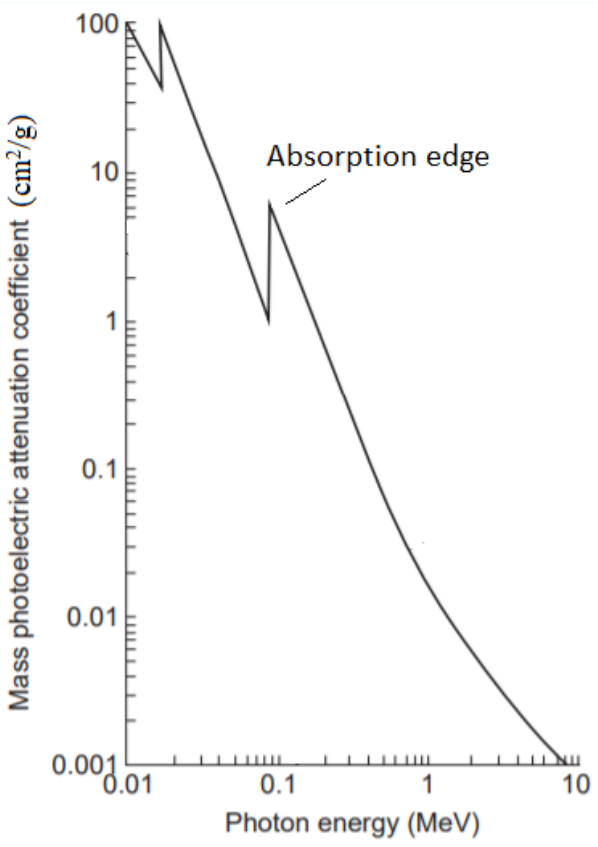

Figure 6. Mass photoelectric attenuation coefficient (μ/ρ) vs energy of the photon for lead. Figure edited from[7].

Discontinuities in a graph corresponds to the binding energies of specific shells and are called absorption edges. Photons branchwith energy less than the particular binding energy are not able to cause the electron emission in that shell and only interactions with higher shells are possible. When energy equals for example K - shell's binding energy the probability of photoelectric attenuation increases dramatically. Between the absorption edges, increasing the photon's energy decreases the probability of interaction until the energy reaches the binding energy of the next shell.[7] Therefore absorption edges reveal the critical values the incoming quanta must have to produce radiation. Along the branches between the absorption edges the attenuation coefficient, μ/ρ, variation is related to the energy of the photon, E_P, and the atomic number, Z, of the absorber according to the equation

$$\mu/\rho = k(\frac{hc}{E_P})^3 Z^3 \ , \tag{6}$$

where k is a specific constant value for each branch. As can be seen from the Equation 6 small energies get absorbed easily while photons with high energies are strongly penetrating. X-rays are termed soft and hard accordingly. Also the atomic number, Z, has similarly strong influence on attenuation of the X-rays in the material.[4, 2]

Filling the vacancy in an excited atom doesn't always lead to the X-ray production. There is also a probability of Auger electron emission. Phenomenon occurs when energy released in filling the empty vacancy is transferred back to a higher orbital electron which is then ejected. In this process the Auger electron has the kinetic energy corresponding the energy difference between the states involved.[7, 2]

The Auger effect is not dependent on the way the atom is ionized. Instead, the atomic number determines its probability, since atoms with low Z, bind electrons more loosely. Therefore, for materials with atomic number less than 31, Auger electron emission is more probable than to emit X-rays. The quantity describing this probability fraction is called the fluorescence yield ω_K and is defined for some shell i

$$\omega_K = \frac{number\ of\ atoms\ emitting\ i\ radiation}{number\ of\ atoms\ with\ a\ i-shell\ vacancy} \ . \tag{7}$$

According to the definition on the Equation 7, the probability for the Auger process is then $(1 - \omega_K)$.[4]

Like stated, the total absorption of the X-ray photons is a combination of the

real absorption, i.e. electronic transitions within the atom, and the scattering of X-rays by the atom. The latter will be discussed in more detail in section 4. However, scattering is not so significant in total absorption except for very light elements.[4]

3.3.2 Filters

In some applications, especially in X-ray diffraction based metallography, it is often necessary or more efficient to attenuate some of the peaks from the spectrum in order to improve the signal-to-noise- ratio for the relevant peaks. This can be done with a filter, made usually from the material with one or two lower atomic number than the X-ray source material. Then the absorption edge of the filter falls example just between the two characteristic peaks absorbing the peak higher in energy.[4] Function of the filter was investigated in the experimental part of this thesis and the illustration of the phenomenon is in the measurement results in Figure 18.

4 X-ray diffraction

In 1912 Mark von Laue discovered the diffraction of X-rays by a crystal lattice. Phenomenon is based on the fact that the wavelength of the X-rays is comparable to the atomic spacing of the lattice. This invention led to new ideas and applications from which one of the most important is the ordered structure of the atomic planes and the resulting Bragg's law.[18]

Diffraction is due to the coherent scattering of the X-rays from the target's electrons and it occurs only in certain directions. Non-coherent scattering also sums up to the scattered intensity as a background radiation and its fraction increases while atomic number decreases.[4, 19]

4.1 Geometrical structure of crystals

A crystal can be defined as a highly organised three dimensional pattern composed of atoms, ions or molecules. The smallest volume, called a unit cell, is defined with three non-coplanar vectors a, b, c for which, when viewed from the point r, can consistently be written $r' = r + u_1a + u_2b + u_3c$, where u_1, u_2 and u_3 are arbitrary integers. The magnitudes of the unit cell vectors and the angles between them are called the lattice constants. These constants are the basis of a total of seven different crystal systems, like cubic and tetragonal, which form 14 different structures, Bravais lattices. Unit cells with atoms only in corners are called the primitive cells and all the rest of the Bravais lattice cells can be defined by them. The 14 Bravais structures are illustrated in Figure 7. In addition, the symmetry operations of the atom arrangements leads to 230 possible space groups.[19, 20]

The structure of crystalline material is based on the continuum of these adjacent unit cells. Every lattice plane can be defined with three, orthogonal lattice vectors, b_1, b_2, b_3 of the basis, $hb_1 + kb_2 + lb_3$ where h,k,l are Miller indices. The Miller index notation is one of the most frequently used to describe the coordinate system of crystals. Usually Miller indices are written so that the highest common divisor is 1. Notation $(hkl) = (hb_1 + kb_2 + lb_3)$ means that the plane (hkl) intercepts the unit cell

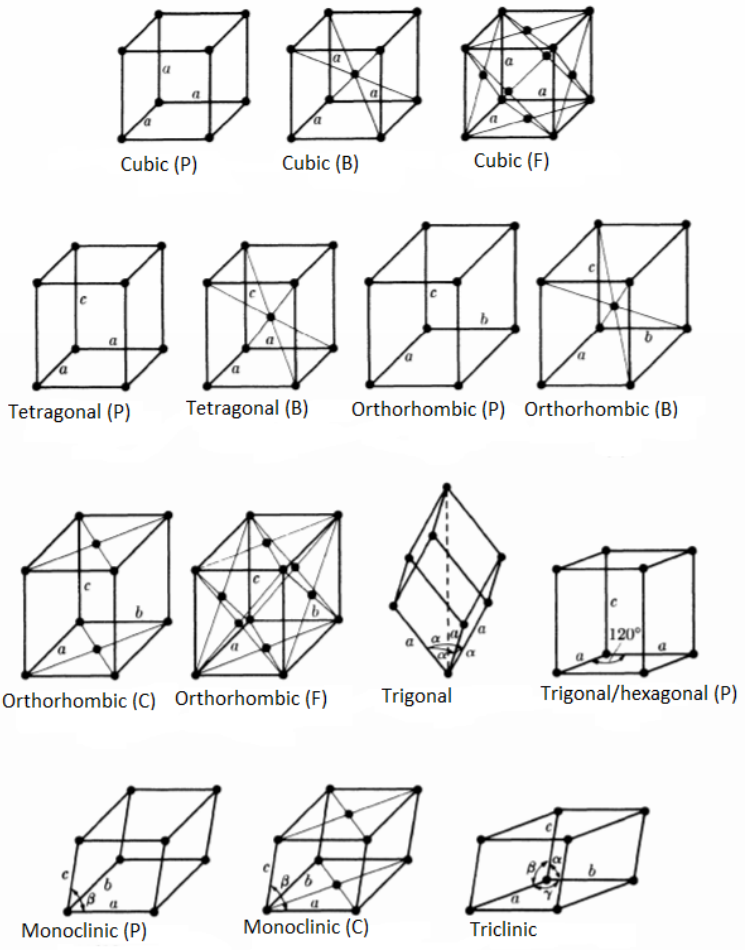

Figure 7. 14 Bravais lattices with lattice constants. P = primitive, C = side-centered, F = face-centered and B = body-centered. Figure edited from [4]

.

at points $(\frac{b_1}{h} + \frac{b_2}{k} + \frac{b_3}{l})$ or some multiple of these. Also the equivalence in symmetry between planes can easily be described with Miller notation (hkl).[19, 20]

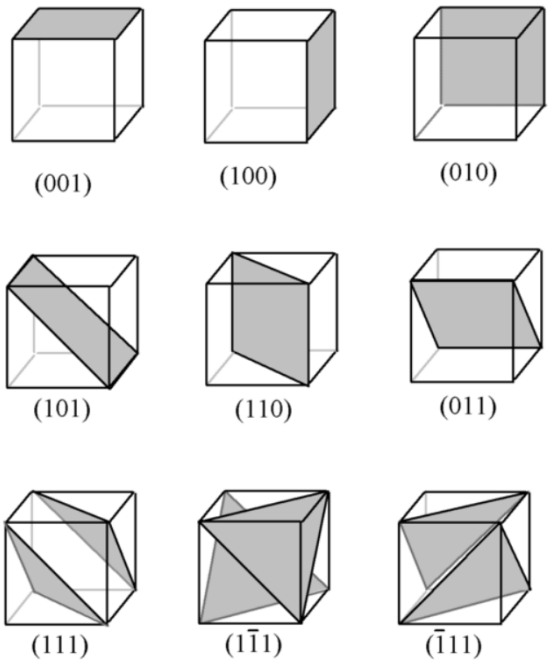

Figure 8. Illustration of Miller notation for cubic cell.[21]

Like stated above, crystalline structure can be expressed using linear combinations of the unit cell vectors. But when it comes to the oblique coordinate systems, the simple rules of vector calculus no longer apply. Reciprocal lattice is defined with new basis which vectors, b'_1, b'_2, b'_3, are both orthonormal and orthogonal to the original basis, b_1, b_2, b_3, and it is often used to simplify the math related to the crystal structure calculations.[19, 20]

4.2 Conditions for diffraction; Laue's and Bragg's laws

Let's consider a beam of X-rays hitting on the material like illustrated in Figure 9. Separate rays scatter from the target's atoms and the phase of a single scattered beam in some point depends both the angle θ of the incident beam and the length of the travelled path. Diffraction occurs only when interference of the rays scattered from different atomic levels in Figure 9 is constructive, meaning 1' and 2' are in the same phase.[22] This condition occurs when the phase difference is the multiple of the wavelength and satisfies the Laue's condition whereby the scattering vector

1'2' ends at the certain point of the reciprocal lattice. This can be illustrated with equation 8

$$1'2' = 2\pi(hb'_1 + kb'_2 + lb'_3) \ , \tag{8}$$

where vectors b'_1, b'_2, b'_3 define a reciprocal lattice of the crystal structure like described in the previous subsection 4.1. Each material has its own specific angle at which the constructive diffraction occurs. θ is then called the Bragg's angle. In some structures the reflected waves attenuate each other and diffraction does not occur at any value of θ.[23]

The spacing d_{hkl} between two planes can be calculated from the magnitude of the reciprocal lattice vector, for example for the cubic lattice, where a is the unit cell vector

$$d_{hkl} = \frac{a}{\sqrt{h^2 + k^2 + l^2}} \ . \tag{9}$$

From the former, Equation 9, we can derive the Bragg's law which is written

$$n\lambda = 2d_{hkl}sin\theta \ , \tag{10}$$

where λ is the wavelength of the incident beam. [24, 22]

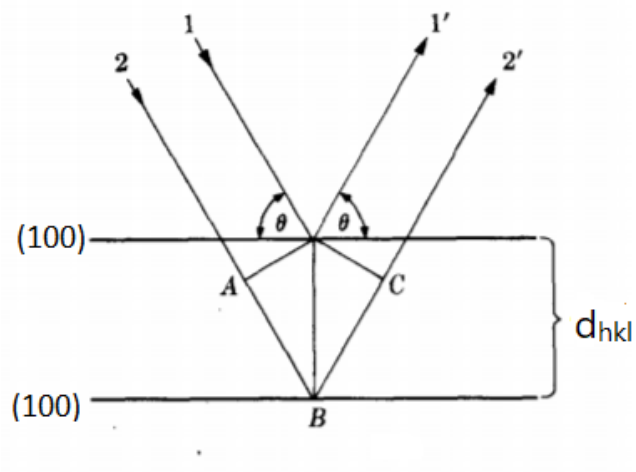

Figure 9. Rays 1 and 2 scatters from different atomic levels of a plane with Miller indices (100). Figure modified from [4].

When keeping the angle of the incident beam constant, all possible diffracted beams draw a construction called the Ewald's sphere. In other words, the scattering

vector must equal with a reciprocal lattice vector. In these terms The Ewald's sphere is very useful predicting the diffraction patterns. While changing the direction of the incoming beam, several Ewald's spheres wrap around the origin of the reciprocal lattice. This reference sphere gives the maximum number of crystal planes which are in a favourable position for diffraction.[25, 22, 23] These geometrical constructions give tools to explain some of the intensity corrections I present in the next subsection 4.3.

4.3 Intensity of the diffracted beam

Sine function can be used to describe the variation of the electric field of propagating X-ray beams.[26] Time-independent intensity calculations for periodically changing sine waves can be derived by using reciprocal lattice and Miller notations.[25, 4] In this subsection I present a few most important results since the goal of this thesis is to get results for which to optimize the X- ray diffraction measurement parameters and intensity calculations are an important aspect when analyzing the diffraction spectrum.

The relative intensity of the diffraction lines is affected by six factors. These are polarization, structure, multiplicity, Lorentz, absorption and temperature factor. In this subsection I present the calculations of the powder diffraction method since it is the most used in X-ray metallography and also in applications of Stresstech Oy. The usability of the method is based on the fact that rarely the measured samples are perfect, single crystals, like described in previous sections but polycrystals instead. Powder method is based on a calibration of a finely grounded and homogenized material which average composition is easy to determine and is comparable to real polycrystalline samples.[25, 4]

The diffraction phenomenon can be explained starting from the intensity of the beam scattered by a single electron in accelerating motion. When taking a square and summing the electric field components of two plane polarized beams, we get the total scattered intensity at some distance R. This is illustrated by the famous Thomson equation

$$\frac{I}{I_0} = (\frac{\mu_0}{4\pi})^2 \frac{e^4}{(m_e)^2}(\frac{1+cos^2 2\theta}{2})\frac{1}{R^2} = K(\frac{1+cos^2 2\theta}{2})\frac{1}{R^2}\ , \tag{11}$$

where $K = 7.94 * 10^{-26} cm^2$ is the classical electron cross section. Thomson formula

contains both the coherent part and the incoherent part, latter corresponding part of the background of a powder diffraction measurement.[25, 4, 27]

Due to the quantum mechanical model for electron distribution of an isolated atom, the electron density $\rho(r)$ is maximum at the nucleus and then falls off as a function of a distance[20]. From the Fourier transform of a density function we get the atomic scattering factor, also known as the form factor f, which describes the "efficiency" of the scattering of a certain atom. Assuming the spherical symmetry, the f depends only on the factor $\frac{\sin\theta}{\lambda}$ which are tabulated for different atoms in several sources. Obviously, for the scattering in forward direction, $f = Z$ for any atom.[25, 4, 26]

The scattering density from the whole crystal lattice structure can be represented by the Fourier series which transform gives us an important quantity, structure factor, F

$$F = \int_V \rho(r) e^{2\pi * i}(h * r) dr \ , \tag{12}$$

where h and r are the reciprocal and real space vectors respectively. Equation 12 gives values which are an "absolute scale" when confining integration over the real space to the unit cell. Another option is to set the scattering density to the atom centers and assign a scattering factor to each one separately. This way we get a sum over N atom positions in the unit cell where vector h is considered with indices (hkl) and r gives the fractional coordinates.[25, 4, 26] The sum can be written

$$F = \sum_{i=1}^{N} f_i e^{2\pi * i}(hu_1 + kv_i + lw_1) \ . \tag{13}$$

When expanding the latter into its trigonometric form with real and imaginary parts separated we get[26]

$$F = \sum_{i=1}^{N} f_i cos(2\pi(hu_1 + kv_i + lw_1)) + i \sum_{i=1}^{N} f_i sin(2\pi(hu_1 + kv_i + lw_1)) \ . \tag{14}$$

Most of the softwares applied for crystallographic structure factor calculations use a simplification based on centrosymmetric arrangement of atoms. This leads to cancellation of the sine term in Equation 14 since the unit cell origin is chosen to position in the inversion center. Two atoms related by certain inversion gets opposite

signs of sine terms.[25, 4]

In real measurements the diffracted intensity consists of reflections also from angles slightly deviating from the Bragg angle. Based on the angle variation, $d\theta$, a reference sphere is used to calculate the number of the favourably oriented planes for diffraction in that specific case as well as the correction for that the diffracted intensity is measured only in one point of the angle-bounded diffraction cone in surface of the sphere. Integrated intensity is a measure which scan over this volume of reciprocal space and gives Lorentz factor, $\frac{cos\theta}{sin^2 2\theta}$, to the intensity equation.[25, 4, 27]

In addition to the factors described above, a few things affecting the diffracted intensity are still worth mentioning. These are absorption, probability for the number of favorably oriented crystal planes, and last, the effect of temperature.

Absorption arises in the material itself and depends strongly on the method used. In the case of a cylindrical specimen a numerical integration over the cross-sectional area with certain absorption coefficient is needed. In a basic powder diffraction method the reflecting planes are usually parallel to each other and the surface and therefore independent of the angle of the incident beam. Absorption factor, $A(\theta)$, gets a constant value.[25, 4]

Multiplicity factor, p, can be defined as a number of permutations of a certain (hkl) plane with equal spacing and structure factor and is therefore dependent on the crystal system geometry. In the other word, p gives a probability factor to which a single (hkl) plane will be correctly orientated for diffraction in a certain crystal structure.[25, 4]

At this point we have assumed atoms to be fixed in one position in the lattice. However, thermal dependent oscillations of lattice atoms decrease the intensity of the diffraction peaks by rising temperature and in turn the background scattering intensifies. Time average of the displacement of the atom from the equilibrium position gives the temperature factor, $e^{-8\pi^2\langle u^2\rangle\frac{sin^2\theta}{\lambda^2}}$, where $\langle u^2\rangle$ is the mean square displacement.[25, 4]

All the factors discussed above can be gathered together into an equation which gives the relative intensity I of powder pattern lines in X-ray diffractometer measurements

$$I = |F|^2 p(\frac{1 + cos^2 2\theta}{sin^2\theta * cos\theta})e^{-2M}(A(\theta)) \ , \tag{15}$$

where M, $-4\pi^2\langle u^2\rangle\frac{sin^2\theta}{\lambda^2}$, is introduced in the previous section.[25, 4]

4.4 Detectors

At the end of the 1940's the first commercially used X-ray spectrometer was developed. The basis of the equipment was the diffraction system(a single crystal) that separates the characteristic photons according to their wavelength which is why the equipment was named wavelength dispersive X-ray spectrometer. In 1966 a significant improvement came to the markets with Li-drifted Si detectors. This new technology provides photon separation without wavelength but is based on the differentiating the photon energies instead. Invention was called the energy dispersive X-ray spectrometer due to its detection system.[16]

Another classification method, in addition to the photon separation, is the counting geometry. Typically three categories are defined based on the detection dimensions. Point, or zero-dimensional, detectors measure the diffraction intensity only a single 2θ position at the time. Due to the counting technology, three most common point detectors are gas proportional, scintillation and semiconductor counters. Latter will be discussed in more detail later since it was the type used in experimental part of this thesis.[28]

Line detectors measure a one-dimensional area of intensity with an array of identical detection elements. Collecting a diffraction pattern from certain 2θ range happens much faster than with a point detector scanning the same line.[28]

Area detectors can measure a distribution of the diffraction intensity in two dimensions. 2D detectors contain detection elements called pixels. This type of detectors are the base and inspiration for many new applications and technologies in X-ray imaging and diffraction.[28]

4.4.1 SDD

Solid-state detectors are based on the ionizations caused by the incoming photon. Each photon produces a certain amount of advancing electron-hole pairs, relative to its energy, which are then registered.

Detector used in this work was a solid-state silicon drift detector, SDD, which utilizes a special drifting technology. The major advance in silicon drift detectors is that they contain a series of ring electrodes that generates a transversal field which

then cause the electron-hole to "drift" to a collection electrode. This technology provides significantly higher count rates due to a lower capacitance, than a conventional semiconductor counter.[29]

4.4.2 Resolution errors

Like stated above resolution of the detector depends on the counting technology. If photons arrive at the detector so close in time that the detection system can't separate them, it may result in errors in the spectrum. Pile-up occurs when the system either records two incoming photons as a single event, in which case the pulse height is a combination of the two, or when photons are spaced further apart they are registered as separate events with incorrect amplitude and energy channel and spectrum becomes blurred. In both cases the spectrum is contaminated and can lead to incorrect results[30].

5 Methods

Experimental part of this work was carried out in a measurement laboratory of Stresstech Oy. The aim was to get comparable results when measuring the X-ray spectra with different values of acceleration voltage and current and with tubes from different manufacturers. Aspects were intensity and clarity of the K_α-peak, the "smoothness" of the spectrum, meaning the amount of pile-up or secondary radiation, and general usability of the tube. The characteristic peaks were identified with X-Ray data booklet[31]. Also attenuation in a material with 0.5 mm Pb equivalent was measured for one of the tubes as well as horizontal limits for the tube target. For the last, diffraction setup was prepared for the Mn-target tube to compare the spectrum to the background. This section goes through the measurement setup, equipment used and finally the measurement methods and results.

5.1 Setup

The measurement setup was constructed into a large cabinet made for robotic X-ray measurements. This ensured the radiation safety of the experiments. Different X-ray tubes were attached to a robotic arm designed for it. The collimator consisted of two parts; a collimator 1 mm in diameter connected to the X-ray tube window approximately 1270 mm from the detector, and a pinhole in a Pb- plate placed 40 mm away from the surface of the detector. The pinhole could be adjusted approximately from 0.3 to 1 mm to control the solid angle of the detector. This made it possible to limit variating count rates. Picture of the setup is in Figure 10.

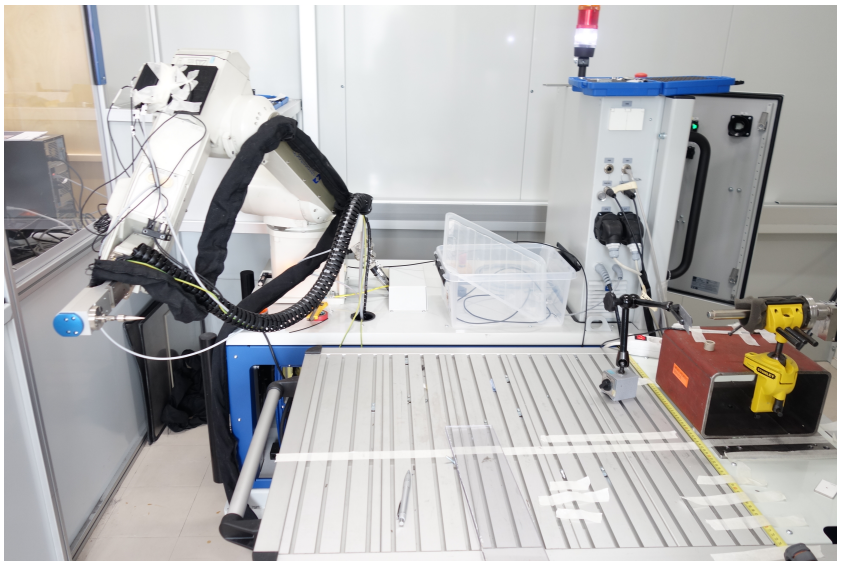

Figure 10. The measurement setup was constructed specifically for the measurements of this thesis. On the left is the robotic arm with one of the tubes and on the right is the detector and the Pb- plate in front of it.

5.2 Equipment

The X-ray tubes used in the measurements were from two different manufacturers, TruFocus and MRX. From the first, tubes with four different target materials; Cr, Cu, Mn and Ti were tested, while from the latter only Cr, Cu and Mn was available. The voltage source was Xtress3000 made by Stresstech Oy and the robotic arm was manufactured by Mitsubishi. The detector used in the measurements was Amptek's XR-100SDD, energy dispersive counter, and it was borrowed from the Acceleration laboratory of the University of Jyvaskyla.

5.3 Data processing

Before I could start analyzing the data I had to calibrate the measured values from the channels of the detector. I plotted the data for each material and found peak maximums with multipeak fitting of GNU Octave software. I set those values as the y-axis and for the x-axis the energies corresponding to the K_α- and K_β-peaks of each material. To the points I fitted a line which equation, $y = 0.00864633 * x - 0.07703166$, I used to convert the values of channel- data into energies. Calibration line and its equation in Figure 11

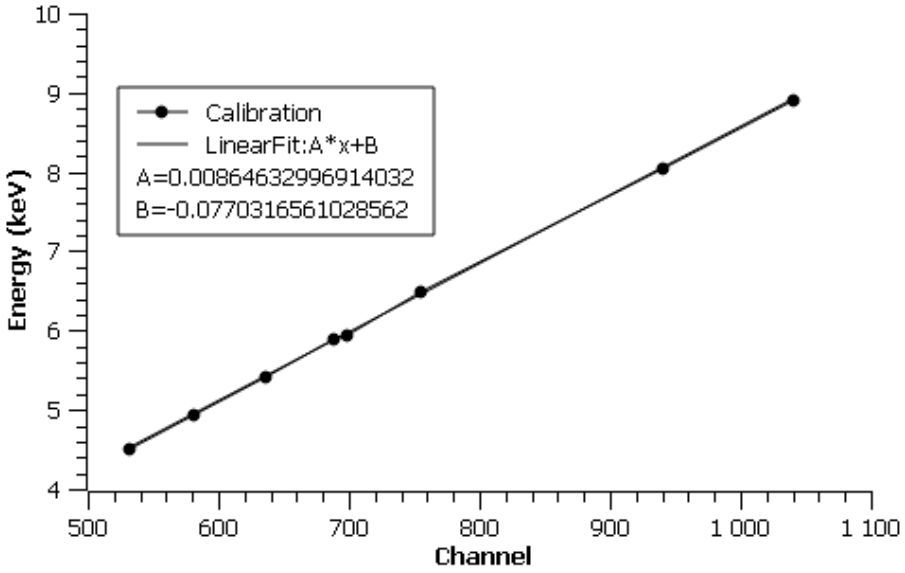

Figure 11. Calibration line for energy conversion of channels.

5.4 Intensity measurements

In this section I first illustrate the effect of air absorption to the intensities of the spectra generated by different photon energies. Second, I present the results for the horizontal measurements to find out the range where the spectrum is properly seen.

Comparing the intensities of the K_α-peaks between tubes straight from the data is not possible since their variation in count rates was so wide that the exposure times and pinhole had to be modified. That's why I have processed each tube's data individually according to the numerical values that fit best for each case. To facilitate the review of the results I have first divided the intensities so that they are comparable to the exposure time point of view and then normalized the data so that the greatest value is 100 and others relative to that. Therefore, I present separate tables consisting of these normalized intensity values for each tube with different values of current and acceleration voltage. In addition, I have plotted the real measured values (not normalized) in logarithmic graphs for some of the measurements to visualize the shape and differences in spectra. The selected acceleration voltage and current values depend on the maximum possible values for each tube and the observations made in the daily laboratory use earlier.

5.4.1 Measurements with varying horizontal position

I carried out measurements where I changed the tube's location by moving the robotic arm in a horizontal direction. Measurements were done with Cr- tube (TruFocus) and with 20 kV acceleration voltage and 6.6 mA current. Location 0 is a spot where no spectrum was seen and other steps are every 5 mm.

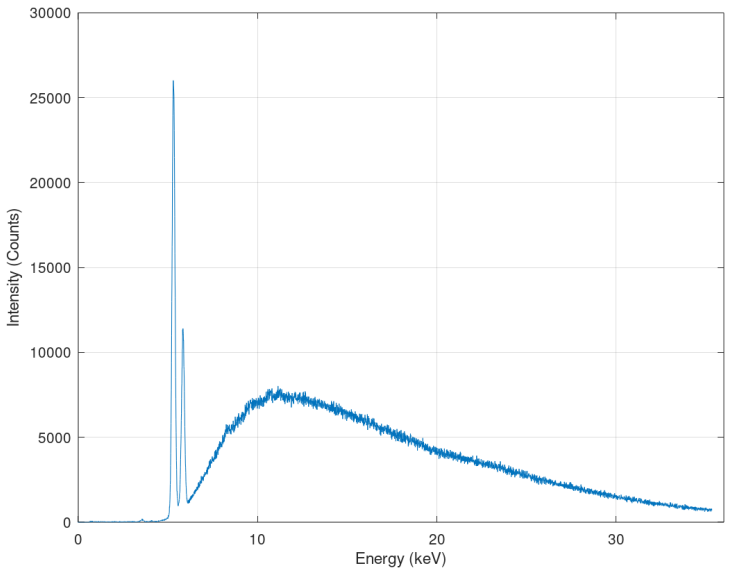

Figure 12. Graph from the horizontal measurements, location 25 mm, where Cr-K_α has the highest intensity.

Table 1. Intensity values when changing the tube position in the horizontal plane.

Location (mm)	Intensity (counts)
0	19
5	26
10	39
15	52
20	12740
25	26020
30	313
35	42
40	30
45	22
50	18

As can be seen from the Table 1 the Cr-K_α- intensity is very strong in a quite narrow space in the horizontal axis and to optimize the intensity of the spectra, the setup should be set exactly in this region. The spectrum from the measurement at the most optimal location, 25 mm from 0, is in Figure 12.

5.4.2 Air absorption

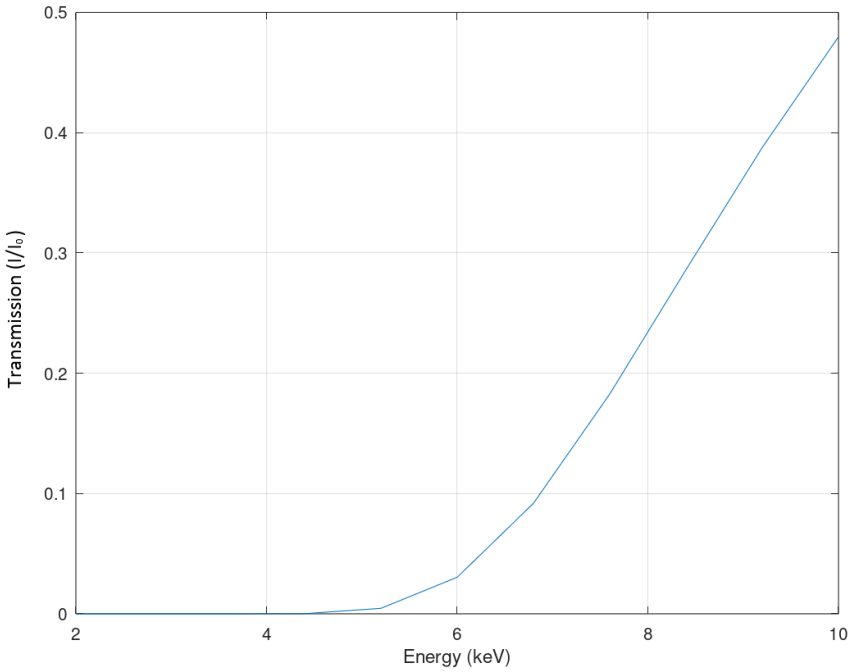

Figure 13. Fraction of transmitted photons in air vs. photon energy. Path was 1270 mm long.

Photon absorption in air can be calculated with exponential attenuation law presented in Equation 2, where the attenuation coefficient μ is unique for each material. In Figure 13, is visualized how the intensity of transmitted photons changes due to the photon energy. The transmission fraction $\frac{I}{I_0}$ was calculated for photon energies from 2 to 10 keV with calculator in the website of The center for X-ray optics [32]. The pressure was set to a normal air pressure 760 Torr and the temperature 293 K from which the application got the μ-values to calculate the transmission fraction. The Table 2 presents the photon transmission fractions for each energy corresponding to the target materials used in this thesis.

As can be seen from the Figure 13 the transmission fraction starts to rise strongly

Table 2. Fraction of transmitted photons in air vs. photon energy.

Material	Energy (keV)	Transmission ($\frac{I}{I_0}$)
Ti	4.51	0.00026
Cr	5.42	0.00850
Mn	5.90	0.025
Cu	8.05	0.25

for photons with energy higher than 5 kV. The X-ray photons generated by different target materials have different energies, and for that reason, significant differences in the transmission to the detector. This mostly explains the need to adjust the pin hole and exposure time.

5.4.3 Tubes with Mn- target

In the intensity measurements for Mn- tubes I first divided the intensity values to correspond to 200 seconds exposure times for both tubes and then normalized them to 0-100 according to the maximum intensity in both cases individually. Tables 3 and 4 shows the normalized intensity values for K_α-peak with values of acceleration voltage 10, 15, 20 kV and currents varying from 1 to 7 mA for MRX and 10, 15, 20, 25 and 30 kV with current range 1 to 6.6 mA for TruFocus. Lower voltage values were measured to see how strong the dependence it has on the intensity.

Count rate with MRX rose that significantly and the pinhole had to be modified during the measurements. Because of this, the intensity values measured with voltage over 20 kV are not comparable and therefore not presented here. In addition each current step from 1 to 7 mA is measured only for the 20 kV due to a tight schedule. With TruFocus one result (10 kV, 5 mA) is missing because of the misfortune in the measurements.

With both of the tubes the normalized intensities increased with increasing acceleration voltage and current. The maximum values of TruFocus were achieved with 30 kV and 6.6 mA which are the upper limits for this tube. The trend was similar for the MRX but as previously noted, the strongly rising count rate prevented the comparison of the results at the higher values.

In Figures 14 and 15 are logarithmic graphs with the real measured values from the measurements with voltages 10 to 30 kV and maximum current. There is clearly seen how the bremsstrahlung changes due to the acceleration voltage. Higher voltage

Table 3. Normalized K_α- intensity values (counts) vs. I,V- values of the Mn-target tube manufactured by MRX.

	10 kV	15 kV	20 kV
1 mA	8.4	7.6	14.4
2 mA	-	-	29.0
3 mA	26.4	22.4	45.9
4 mA	-	-	64.6
5 mA	40.0	39.0	79.5
6 mA	-	-	81.3
7 mA	54.0	54.3	100

Table 4. Normalized K_α- intensity values (counts) vs. I,V- values of the Mn-target tube manufactured by TruFocus.

	10 kV	15 kV	20 kV	25 kV	30 kV
1 mA	0.9	3.9	7.5	11.7	15.1
3 mA	2.6	10.7	21.2	30.7	35.1
5 mA	-	16.8	32.5	43.2	71.2
6.6 mA	5.3	21.7	40.3	66.5	100.0

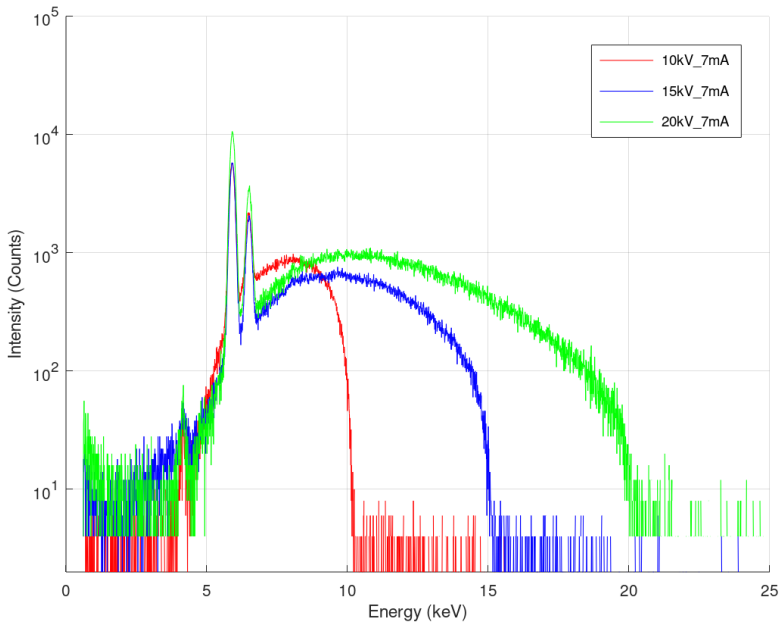

Figure 14. Real measured K_α- intensity values with maximum currents and varying voltages in logarithmic scale vs. photon energy for Mn-target tube manufactured by MRX.

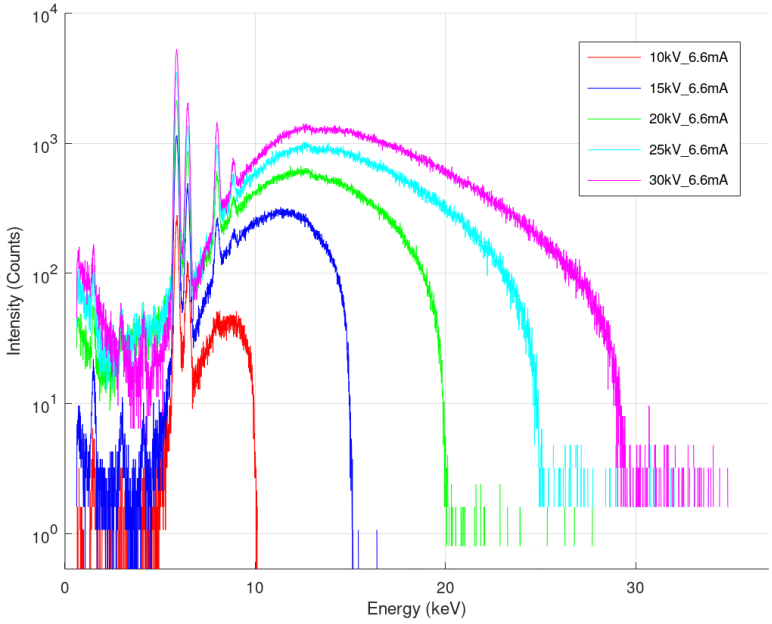

Figure 15. Real measured K_α- intensity values with maximum currents and varying voltages in logarithmic scale vs. photon energy for Mn-target tube manufactured by TruFocus.

increase the endpoint energy while low energy branch stays constant. In addition, the lower energy region contains propably secondary radiation in a case of both of the tubes. Spectra from the measurement of TruFocus contains peaks with energy of copper which is probably because the tube has worn out.

5.4.4 Tubes with Cr- target

As was done in the case of copper I first divided the intensity values to correspond to 200 seconds exposure times for both Cr-target tubes and then normalized them to 0-100. Tables 5 and 6 shows the normalized intensity values for K_α-peak with different values of acceleration voltage (27-30 kV) and current (1-9 mA).

With TruFocus the measurements went well. I carried out measurements from 20 to 30 kV with 1 kV steps and each step with current values 1-9 mA. With lower parameters intensities were clearly lower, accordingly, with no exceptions. I therefore present results only from 27 kV because they are the most interesting values since they produce intensity high enough for practical XRD measurements and also coincide with the scale of the parameters used in the measurements with MRX.

Table 5. Normalized K_α- intensity values (counts) vs. I,V- values of the Cr-tube manufactured by TruFocus.

	27 kV	28 kV	29 kV	30 kV
1 mA	9.4	10.6	10.7	11.2
2 mA	15.6	16.5	20.6	21.6
3 mA	24.1	28.1	33.0	33.9
4 mA	37.6	41.8	44.6	45.5
5 mA	48.1	51.5	55.4	56.0
6 mA	56.8	62.5	65.0	69.6
7 mA	67.6	72.8	76.5	80.5
8 mA	77.6	82.8	91.1	92.4
9 mA	88.2	93.4	99.8	100.0

Table 6. Normalized K_α- intensity values (counts) vs. I,V- values of the Cr-tube manufactured by MRX.

	27 kV	28 kV	29 kV	30 kV
1 mA	12.3	12.7	13.9	13.7
2 mA	23.4	24.3	26.4	26.4
3 mA	33.4	36.2	37.7	40.8
4 mA	43.3	46.7	48.1	53.4
5 mA	51.4	59.5	60.1	63.4
6 mA	59.7	66.4	74.4	71.6
7 mA	67.5	74.3	79.8	81.9
8 mA	76.7	82.1	88.8	90.3
9 mA	85.4	87.2	91.3	100.0

At high current values a breakthrough current occured in MRX- tube. This may be due to a poor cooling system of the tube which causes the current breakthrough as temperature rises. After a few failed measurements I tried to start from the upper limit of the current in each voltage step and measure downwards to lower values. This helped to keep the tube in function and I got the measurements done.

As can be seen from the Tables 5 and 6 the intensity values increase with increasing voltage and current. With TruFocus there is actually no difference whether the voltage is 29 or 30 kV with maximum current but with MRX the normalized intensity value is approximately 10 percent smaller with 1 kV lower voltage. The voltage dependence is also illustrated in Figures 16 and 17.

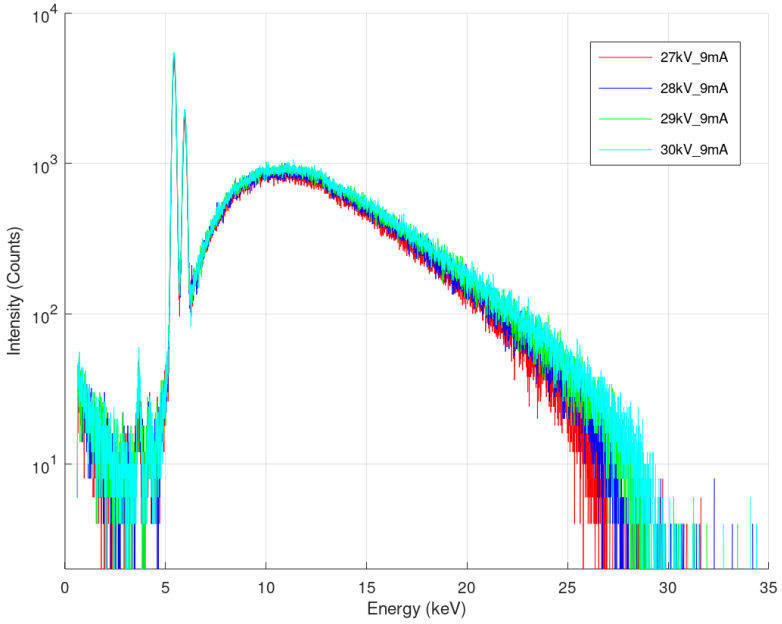

Figure 16. Real measured K_α- intensity values in logarithmic scale vs. photon energy for Cr-target tube manufactured by TruFocus.

For the Trufocus I carried on also measurements with a vanadium (V) filter with maximum values of voltage and current (30kV, 9mA). Vanadium has atomic number one lower than chromium[33] and its K- absorption edge falls right between Cr- K_α- and -K_β-peaks. As a result, the whole spectrum attenuates but the intensity of the K_β-peak decreases relatively most. The effect of the filter can be seen from the Figure 18 where the red graph is spectra without, and the blue with filter.

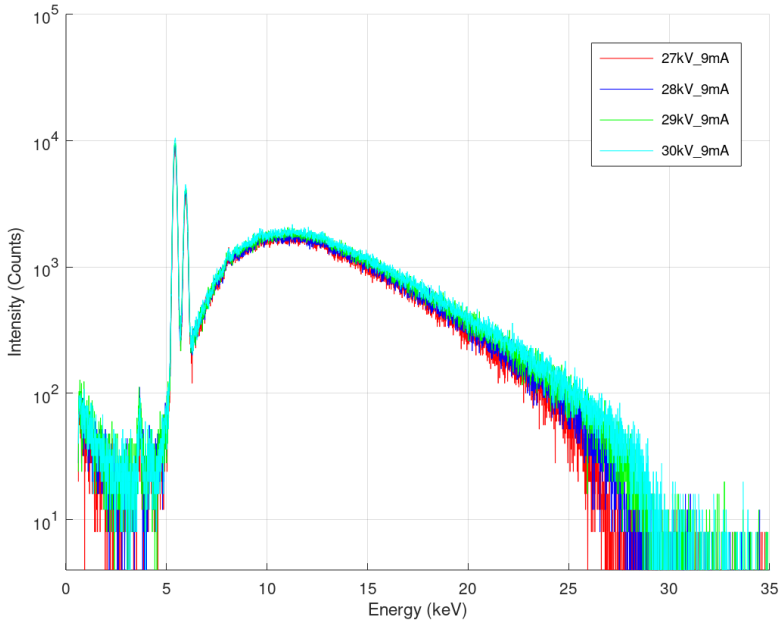

Figure 17. Real measured K_α- intensity values in logarithmic scale vs. photon energy for Cr-target tube manufactured by MRX.

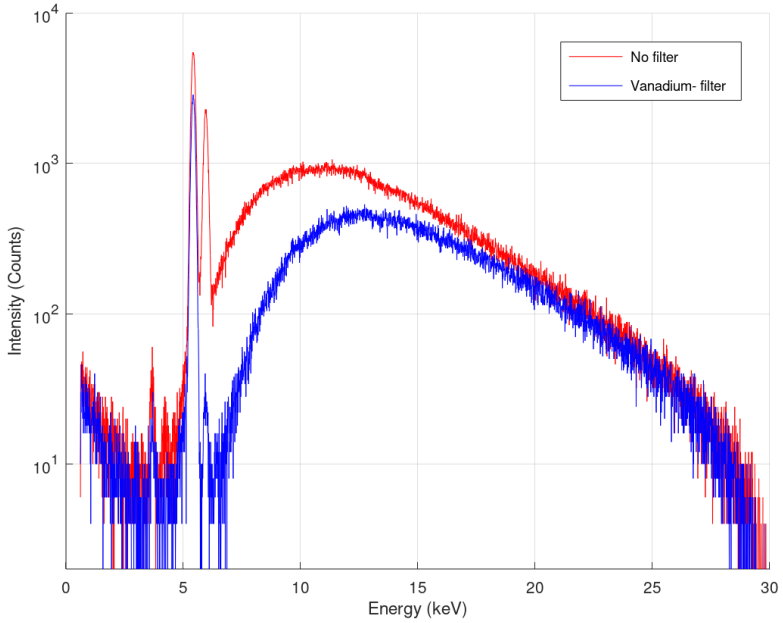

Figure 18. Locarithmic intensity values from the measurement of the Cr- target tube without (red) and with (blue) vanadium filter. 30 keV acceleration voltage and 9 mA current was used in both of the measurements.

5.4.5 Tubes with Cu- target

With Cu- tubes the exposure times were also modified to 200 seconds and intensity values normalized to 0-100. The acceleration voltages were 10, 15, 20, 25 and 30 kV with 1, 3, 8, and 10 mA currents. For the MRX- tube also currents from 9 to 10 mA were measured with 0.1 mA steps to investigate the high and unexpected decrease in intensity observed in previous measurements not related in this thesis. As can be seen from the Tables 8 and 9, a very clear deviation from the rest of the data is at a current value of 9.5 mA and rest of the normalized intensity values are significantly lower. This deviation can be explained either by a property of the tube or some malfunction in the generator or in the tube itself. If it were a property, it would be a significant consideration in the XRD measurements. Also TruFocus was measured in the highest voltage (30 kV) with 9 mA to see if there is any difference compared to 10 mA current.

Measurements with TruFocus went without any complications like Table 7 shows. Also the results were as expected meaning the normalized intensity values increased according to the measurement parameters and reached its maximum value with 30 kV and 10 mA.

Table 7. Normalized K_α- intensity values (counts) vs. I,V- values of the Cu-tube manufactured by TruFocus.

	10 kV	15 kV	20 kV	25 kV	30 kV
1 mA	0.1	1.2	3.1	5.3	7.6
3 mA	0.2	3.3	9.2	17.4	24.3
8 mA	0.7	8.0	28.0	49.4	72.0
9 mA	-	-	-	-	83.7
10 mA	0.9	13.2	61.2	64.6	100

Table 8. Normalized K_α- intensity values (counts) vs. I,V- values of the Cu-tube manufactured by MRX.

	10 kV	15 kV	20 kV	25 kV
1 mA	0.1	1.1	2.4	3.6
3 mA	0.1	1.9	3.8	5.8
8 mA	0.1	1.8	3.7	5.4
10 mA	0.1	1.6	3.3	5.0

Table 9. Normalized K_α- intensity values (counts) with 30 kV and currents 9 - 10 mA, 0.1 mA steps vs. power of the Cu-tube manufactured by MRX.

	30 kV
1 mA	4.0
3 mA	7.3
8 mA	9.3
9 mA	15.2
9.1 mA	18.7
9.2 mA	23.2
9.3 mA	34.8
9.4 mA	49.0
9.5 mA	100
9.6 mA	68.9
9.7 mA	11.9
9.8 mA	13.2
9.9 mA	9.3
10 mA	9.1

Measured intensity values in logarithmic scale as a function of the voltage with maximum currents are illustrated in Figures 20 and 21 where it can be seen that the emission of the bremsstrahlung radiation in copper target is also highly dependent of the voltage.

In addition the attenuation of the radiation was measured with a Cu- tube (TruFocus) when a shielding plex was set between the tube and the detector, approximately 300 mm from the detector. The Mavig- plex used in the measurement has 0.5 mm Pb- equivalent which corresponds to the thin plate in front of the detector. The plex tested, absorbed almost all of the emitted radiation, Figure 19, when measuring with 30 kV and 10 mA. This test shows us two things. First, Mavig- plex is usable as a radiation shield material in the measurements with this energy region. Second, in the measurements, radiation passed to the detector only through the pinhole and the flux was smooth from that aspect. If the comparison between tubes had been made, the change in count rates could have been calculated by the change in the diameter of the pinhole.

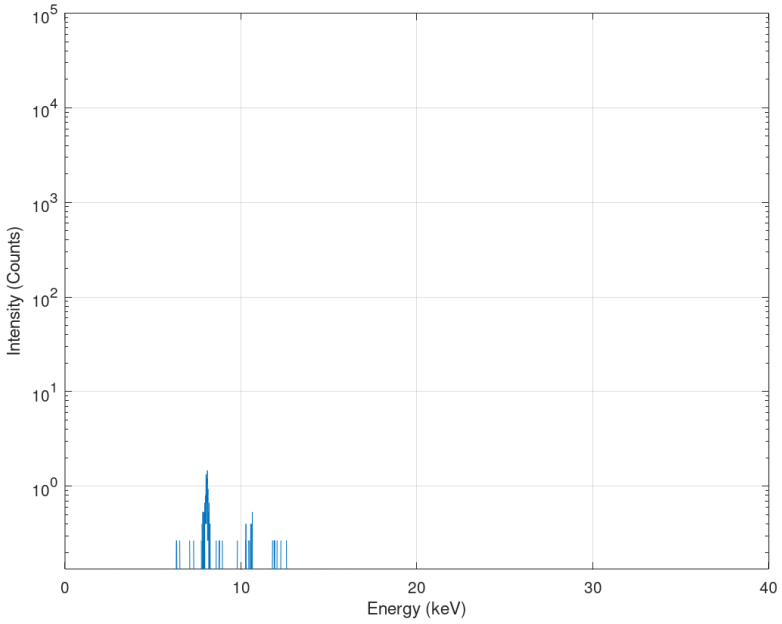

Figure 19. Measured intensity in logarithmic scale when 0.5 mm Pb- equivalent Mavigplex- shield was was set between the tube and the detector. 30 kV acceleration voltage and 10 mA current was used in the measurement.

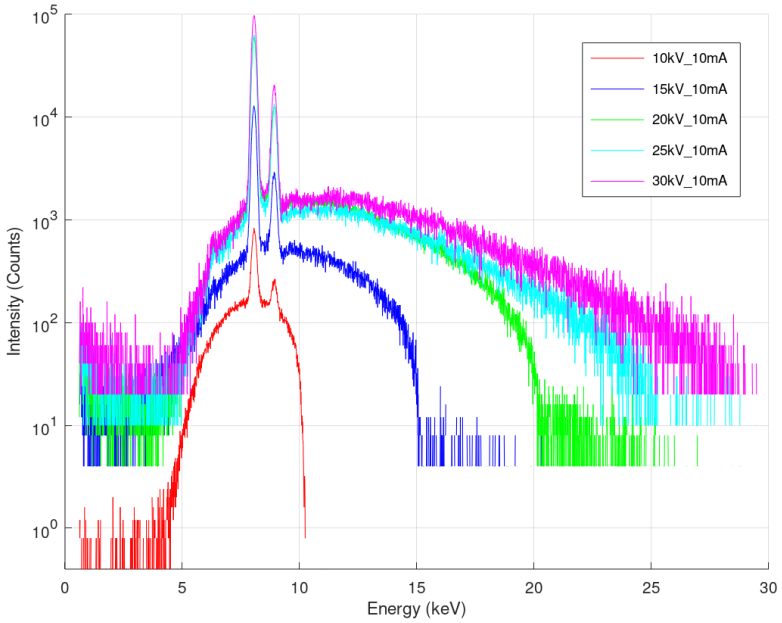

Figure 20. Real measured K_α- intensity values in logarithmic scale vs. photon energy for Cu-target tube manufactured by TruFocus.

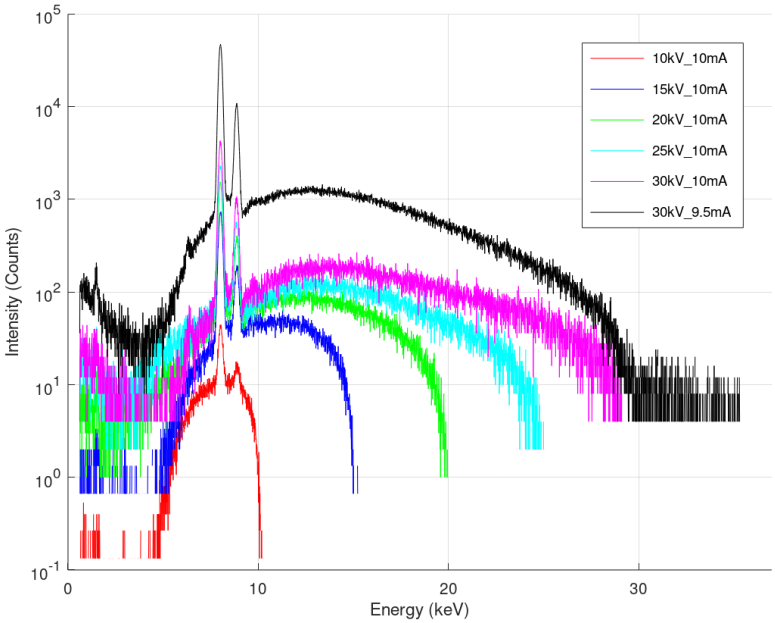

Figure 21. Real measured K_α- intensity values in logarithmic scale vs. photon energy for Cu-target tube manufactured by MRX.

5.4.6 Tube with Ti- target

Tube with Ti- target was tested only with TruFocus. With titanium, the problem has been relatively long exposure times. Spectra with logarithmic intensity scale in Figure 22 reveals that the bremsstrahlung radiation has significantly higher maximum intensity than the characteristic radiation. The background radiation will be deducted with intensity calculations in XRD measurements but to get the signal-to-noise-ratio good enough for the characteristic peak the long exposure time is needed, usually many times longer than for example tube with Cr- target.

Measurements were carried out with voltages 28, 29 and 30 kV which were expected to produce the highest intensity values. Each voltage step was measured with 1, 2, 4, 6 and 8 mA currents. Exposure times were aligned to 800 seconds and intensity values normalized to 0-100. As can be seen from the Table 10 normalized intensity gets higher values with higher measurement parameters as can be expected.

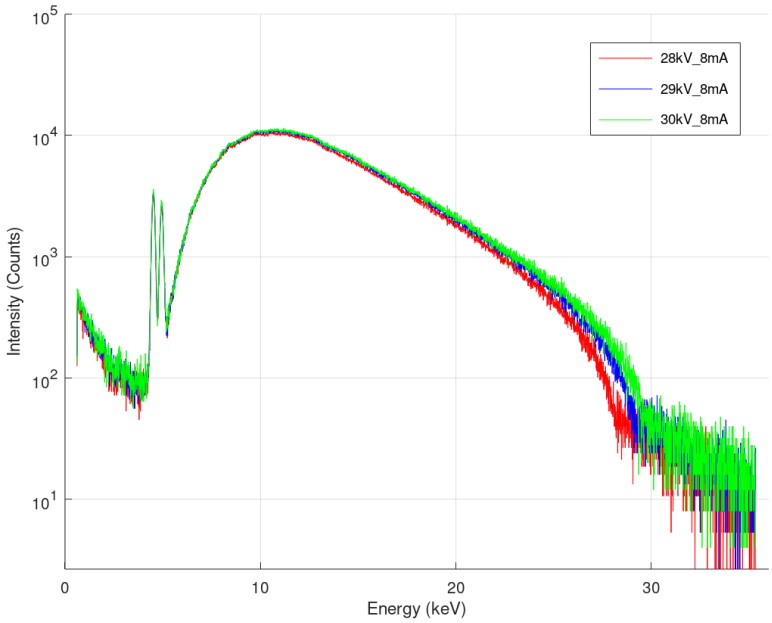

Figure 22. X-ray spectra for real measured intensity values of Ti-target tube with maximum current and acceleration voltages from 28 to 30 kV.

Table 10. Normalized K_α- intensity values vs. I,V- values of the Ti-target tube manufactured by TruFocus.

	28 kV	29 kV	30 kV
1 mA	12.1	12.1	12.5
2 mA	21.7	24.0	24.6
4 mA	45.0	46.3	44.7
6 mA	69.3	69.6	70.9
8 mA	92.0	94.9	100.0

5.5 Diffraction measurements

For the last measurement I built a setup to visualize the diffraction laws introduced in section 4. I had the Mn- tube (MRX) attached to the robotic arm and in front of that, approximately 5 mm away from the collimator, I set a austenitic steel powder sample. I placed the detector to 152 degrees from the horizontal plane of the sample according to the diffraction angle which is used in Stresstech's laboratory measurements for austenitic steel powder. Acceleration voltage was 25 keV and current 6.6 mA. Setup is seen on the Figure 23.

Powder sample used is of alloy AISI 347 composition and it has a face-centered cubic construction. It's iron based and contains at least 10.5% chromium. In addition, the compound includes some amount of nickel and niobium.[34]

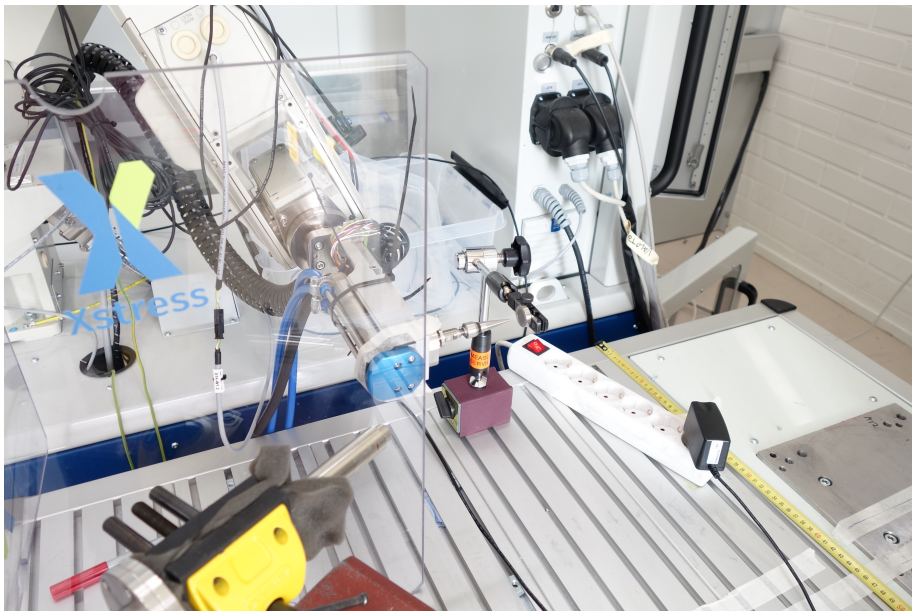

Figure 23. Diffraction measurement setup. The powder sample is a small, round piece in front of the collimator. In the forefront of the Figure is the detector placed in 152 degrees relative to the sample surface. Acceleration voltage was 25 keV and current 6.6 mA.

First I measured only air without the sample to see the background. As expected, only weak Mn- peaks were seen in the background spectrum. In the powder sample measurement the spectrum contained several peaks with relatively high intensity. Figure 24 shows both spectra with logarithmic intensity- axis. The lowest in energy is probably the Cr- K_α and the second is the sum of the Mn- K_α and Cr- K_β. Energy approximately 6.4 keV can be combination of the Mn- K_β and the Fe- K_α while 7

kV fits for the energy of the Fe- K_β. The highest peaks correlate with the energy of the K_α and the K_β of nickel.

The several peaks in the spectrum are probably, and mostly, due to the fluorecence phenomenon. However, spectrum contains indications about diffraction. Powder sample doesn't contain any manganese but the spectrum has significant increase in the intensity of the K_α- and the K_β-peaks of manganese. This may be a consequence of the summation of the reflected beams from different crystal levels of the powder sample. For example, the wavelength corresponding to the energy of the Mn-K_α is suitable for diffraction of the Cr-K_β-peak. This is why the Cr-K_β has higher intensity compared to K_α even the latter should have intensity at least couple times higher.

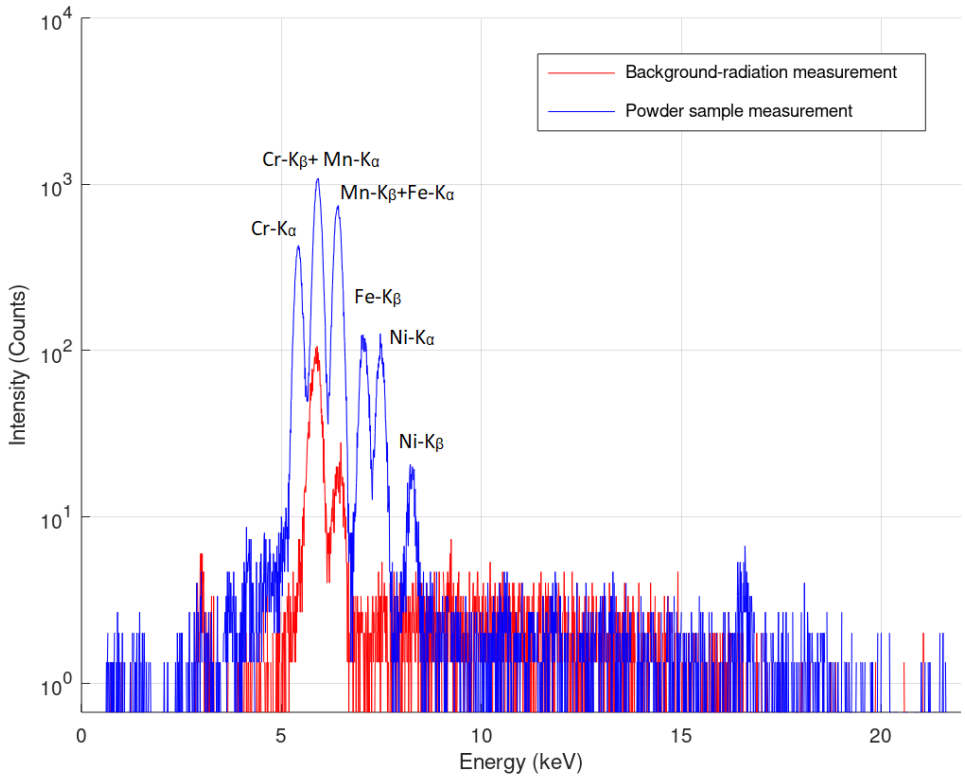

Figure 24. The spectra from the background (red) and powder sample (blue) measurements with Mn- target tube.

6 Conclusions

In this thesis I studied properties of X- ray tubes with different target materials from two different manufacturers to make comparison between them and to improve the practical measurements in the laboratory. I carried out the measurements with different acceleration voltages and currents from lower values to the top limits of each tube.

Results were mainly as expected; count rates increased among increasing values of voltage and current. Unfortunately, intensities are not directly comparable to each other. As shown in subsection 5.4.2, the air absorption of the radiation produced by different target materials varies greatly. If the exposure time and pinhole had not been changed, some of the measurements would have taken days. Especially Cu-target tubes, and to some extent also copper, produced pile-up and secondary radiation which are usually most common with higher count rates. On the other hand, low count rates would cause the intensity of the characteristic peaks to remain far too low to separate them from the background. Despite these effects, some important observations can be done.

With the Cr-target tube from TruFocus there was no difference in the spectrum whether 29 or 30 kV acceleration voltage was used. Lower voltage decreases the heat formation and saves both the tube and energy. When tubes are used for hundreds of hours a year, even a relatively small decrease in voltage can extend the lifetime of the tube. Also lower value of voltage would be better from the radiation safety point of view since photons with smaller energies have a weaker penetration ability for shielding materials. Although, this effect is quite insignificant in energies at this range.

Characteristic radiation of titanium has the lowest energy from studied tube materials. This was seen in the spectrum as significantly higher intensity of the bremsstrahlung compared to the characteristic peaks. This is explained by the fact that fewer electrons have just the right energy to ionize the targets atoms. Also the air absorption is considerably stronger with lower energy photons. Therefore, with titanium increasing the voltage does not significantly improve the signal-to-noise-ratio

of the characteristic peaks, but the longer exposure time does.

Some general observations about the function of the tubes were that TruFocus was, at least based on this study, more reliable. MRX- tubes had problems such as current breakthroughs caused by the temperature rise. However, the study was so narrow that nothing completely certain can be said.

The last subject of this thesis was diffraction measurements which remained without the attention I would have liked to give. The detector was set exactly in that specific angle which was known to produce diffraction from the crystal levels of the measured austenitic steel powder sample. When compared to the background, there were clearly more peaks with higher intensity. Most of the intensity of these peaks is probably explained by the fluorecence but in a case of the peaks which energy correlate to the target's energy can be indication of diffraction. From the spectrum in Figure 24 can be seen that Cr-K_α- has lower intensity than K_β-peak even the first should have intensity at least two or three times higher. This can be explained by the laws described in section 4. The initial waves coming from the source sums up from the crystal levels of the powder sample. The wavelength of the inital wave is suitable relative to powder sample's atomic level distance for constructive interference to occur. However, more measurements would be required to verify the phenomenon.

In general, the measurements went well, but the tight schedule posed challenges and forced to leave out some of the planned measurements. In the future it would be possible to do studies with tubes from several different manufacturers and improve the setup so that the intensities would be more comparable. This could be done either by adjusting the pinhole so that the change in the radiation flux could be accurately calculated. Another option could example be to adjust the distance between the tube and the detector in a way that the air absorption would be equal for different target materials.

However, the results of this thesis prove that even relatively small differences in measurement parameters like acceleration voltage, current or exposure time could affect the intensity of the characteristic peaks, especially the K_α-peak, which is crucial in XRD measurements. On the other hand, a small decrease in the acceleration voltage can increase the lifetime of the tube. Finding the balance between these aspects would enhance the optimization and efficiency of the XRD measurements.

References

[1] W. C. Röntgen. "On a new kind of rays". In: *Science 3.59(1896), 227-231* (Sept. 23, 2010). URL: https://www.jstor.org/stable/1623595 (visited on 09/18/2020).

[2] D.McMorrow J. Als-Nielsen. *Elements of modern X-ray physics*. 2nd ed. John Wiley and Sons, Inc., 2011. URL: https://ebookcentral.proquest.com/lib/jyvaskyla-ebooks/reader.action?docID=699505 (visited on 09/08/2020).

[3] Randall.D.Knight. *Physics for Scientists and Engineers: A Stratetic Approach with Modern Physics*. 4th ed. Pearson Education, 2017.

[4] B.D.Cullity. *Elements of X-Ray Diffraction*. 2nd ed. Addison-Wesley Publishing Company, Inc., 1978.

[5] *NASA, Imagine the universe*. URL: https://imagine.gsfc.nasa.gov/science/toolbox/emspectrum1.html (visited on 09/25/2020).

[6] J. Selman. *The Basic Physics of Radiation Therapy*. 3rd ed. Charles C Thomas Publisher, 1990.

[7] F. M. Khan. *The Physics of Radiation Therapy*. 4th ed. Lippincott Williams and Wilkins, a Wolters Kluwer business, 2010.

[8] I. Buvat C. Grupen. *Handbook of particle detection and imaging*. 2nd ed. London, New York: Springer-Verlag Berlin Heidelberg, 2012.

[9] J.Fernández-Varea F. Salvat and et al. "PENELOPE-2011: A Code System for Monte Carlo Simulation of Electron and Photon Transport". In: *NEA Data Bank, Workshop Proceeding* (July 2011).

[10] J. H. Hubbel. "Photon Cross Sections, Attenuation Coefficients, and Energy Absorption Coefficients from 10 keV to 100 GeV". In: *Natl Standards Reference Data System Natl Bureau of Standards 29* (Aug. 1969). URL: https://nvlpubs.nist.gov/nistpubs/Legacy/NSRDS/nbsnsrds29.pdf (visited on 10/03/2020).

[11] P-G. Rancoita C. Leroy. *Principles Of Radiation Interaction In Matter And Detection*. 3rd ed. Singapore: World Scientific., 2012. URL: http://web.b.ebscohost.com.ezproxy.jyu.fi/ehost/ebookviewer/ebook/bmxlYmtfXzQyNjQ1MF9fQU41?sid=f71cd6ef-93d3-424b-ba32-315d21757dca@sessionmgr103&vid=0&format=EB&rid=1 (visited on 06/14/2020).

[12] T. Jerrold. Bushberg. *The Essential Physics of Medical Imaging*. 3rd ed. Wolters Kluwer Health/Lippincott Williams and Wilkins, 2012.

[13] *NASA's HEASARC*. URL: https://heasarc.gsfc.nasa.gov/docs/heasarc/headates/spectrum.html (visited on 10/03/2020).

[14] G. V. Pavlinsky. *Fundamentals of X-ray Physics*. Cambridge International Science Publishing, 2008.

[15] *Lumen learning*. URL: https://courses.lumenlearning.com/physics/chapter/30-4-x-rays-atomic-origins-and-applications/ (visited on 10/28/2020).

[16] R. Grieken E. Marguí. *X-ray fluorescence spectrometry and related techniques: An introduction*. New York: Momentum Press, 2013.

[17] E. B. Podgoršak. *Energy Transfer and Energy Absorption in Photon Interactions with Matter. In: Radiation Physics for Medical Physicists*. Springer-Verlag Berlin Heidelberg, 2009.

[18] K. Shih. *X-ray diffraction: Structure, principles and applications*. Nova Science Publishers, Inc., 2013. URL: http://search.ebscohost.com.ezproxy.jyu.fi/login.aspx?direct=true&db=nlebk&AN=632991&site=ehost-live (visited on 09/08/2020).

[19] C. Kittel. *Introduction to solid state physics*. 7th ed. USA: John Wiley and Sons, Inc., 1996.

[20] H. Lüth H. Ibach. *Solid-state physics : an introduction to principles of materials science*. 4th ed. New York: Springer cop., 2009.

[21] *NanoWireWiki*. URL: http://nano-physics.pbworks.com/w/page/12296660/FrontPage (visited on 09/10/2020).

[22] E. Wolf M. Born and et al. *Principles of optics : electromagnetic theory of propagation, interference and diffraction of light*. 7th ed. Cambridge: Cambridge University Press cop., 1999.

[23] R. Dick. *Advanced quantum mechanics: Materials and photons*. 1st ed. New York: Springer, 2012.

[24] J. Cooper D. Sherwood. *Crystals, X-rays and Proteins: Comprehensive Protein Crystallography*. Oxford: OUP Oxford, 2011. URL: http://search.ebscohost.com.ezproxy.jyu.fi/login.aspx?direct=true&db=nlebk&AN=1069276&site=ehost-live (visited on 07/21/2020).

[25] R. E. Dinnebier S. J. L. Billinge. *Powder diffraction: Theory and practice*. 3rd ed. Cambridge, U.K.: Cambridge: Royal Society of Chemistry, 2012. URL: http://search.ebscohost.com.ezproxy.jyu.fi/login.aspx?direct=true&db=nlebk&AN=496238&site=ehost-live (visited on 08/04/2020).

[26] J. F. James. *A student's guide to fourier transforms: with applications in Physics and engineering*. 2nd ed. Cambridge, U.K.: Cambridge University Press, 2002. URL: http://web.a.ebscohost.com.ezproxy.jyu.fi/ehost/ebookviewer/ebook/bmxlYmtfXzEyNTA3M19fQU41?sid=3248f5b2-b72c-498f-845b-31ba785f803c@sessionmgr4006&vid=0&format=EB&rid=1 (visited on 08/17/2020).

[27] D. S. Sivia. *Elementary scattering theory: For X-ray and neutron users*. Oxford: OUP Oxford, 2011.

[28] B. B. He. *Two-dimensional x-ray diffraction*. 1st ed. John Wiley and Sons, Inc., 2009. URL: https://ebookcentral.proquest.com/lib/jyvaskyla-ebooks/reader.action?docID=469502 (visited on 08/17/2020).

[29] F. G. Knoll. *Radiation detection and measurement*. 3rd ed. New York: John Wiley and Sons, Inc., 1999. URL: https://phyusdb.files.wordpress.com/2013/03/radiationdetectionandmeasurementbyknoll.pdf (visited on 09/04/2020).

[30] E. C. Frey K. Taguchi and et al. "An analytical model of the effects of pulse pileup on the energy spectrum recorded by energy resolved photon counting x-ray detectors". In: *Medical physics, 37(8), 3957–3969* (July 12, 2010). URL: https://www.ncbi.nlm.nih.gov/pmc/articles/PMC2917451/ (visited on 09/18/2020).

[31] *X-Ray data booklet*. URL: https://xdb.lbl.gov/ (visited on 09/16/2020).

[32] *CXRO, The center for x-ray optics*. URL: https://henke.lbl.gov/optical_constants/ (visited on 09/15/2020).

[33] *Ptable*. URL: https://ptable.com/?lang=fi#Ominaisuudet (visited on 09/16/2020).

[34] *Goodfellow*. URL: http://www.goodfellow.com/E/Stainless-Steel-AISI-347.html (visited on 10/29/2020).